Transient Incomplete Separation Facilitates Finding Accurate Equilibrium Dissociation Constant of Protein–Small Molecule Complex

*Nicolas Sisavath, Jean Luc Rukundo, J. C. Yves Le Blanc, Victor A. Galievsky, Jiayin Bao, Sven Kochmann, Alexander S. Stasheuski and Sergey N. Krylov**

Abstract: *Current practical methods for finding the equilibrium dissociation constant, K_d, of protein–small molecule complexes are mainly biosensoric and calorimetric. They have inherent sources of inaccuracy; immobilization of molecules on sensors and heat of side reactions often lead to dramatic errors in K_d. We introduce "accurate constant via transient incomplete separation" (ACTIS), a non-biosensoric and non-calorimetric approach for finding K_d, which appears to be free of inherent sources of inaccuracy. Conceptually, in ACTIS, a short plug of the pre-equilibrated protein–small molecule mixture is pressure-propagated in a capillary, causing fast transient incomplete separation of the complex from the unbound small molecule. A superposition of signals from these two components is measured near the capillary exit and used to calculate a fraction of unbound small molecule, which, in turn, is used to calculate K_d. In this work, we prove ACTIS validity theoretically, verify its accuracy by computer simulation, and demonstrate its practical use. Owing its suggested accuracy, ACTIS has a potential to become a reference-standard method for finding K_d of protein–small molecule complexes.*

Reversible binding of proteins (P) to small-molecule ligands (L) plays an important role in regulation of cellular processes.[1] In addition, most therapeutic targets are proteins,[2] and drugs are developed to form stable PL complexes with them:

$$\mathrm{P} + \mathrm{L} \rightleftharpoons \mathrm{PL} \quad (1)$$

Complex stability is characterized by the equilibrium dissociation constant K_d which is defined as:

$$K_d = [\mathrm{L}]_{eq}[\mathrm{P}]_{eq} / [\mathrm{PL}]_{eq} \quad (2)$$

where $[\mathrm{P}]_{eq}$, $[\mathrm{L}]_{eq}$, and $[\mathrm{PL}]_{eq}$ are equilibrium concentrations of P, L, and PL, respectively. Finding accurate K_d values of PL is pivotal for creating adequate models in systems biology and correctly ranking pharmaceutical hits in early stages of drug development.[3]

All established methods for finding K_d of PL known to us have inherent sources of inaccuracy. Fluorescence spectroscopy and thermophoresis require labeling L with a fluorophore, which affects L's binding to P and, thus, the accuracy of K_d measurements;[4] these techniques cannot be combined with other than fluorescence modes of detection. Biosensoric techniques require the immobilization of either L or P onto a sensor surface, which also affects binding and, thus, accuracy of K_d measurements.[5] Isothermal titration calorimetry does not require labeling or immobilization but has another source of inaccuracy: the heat of side reactions (e.g. binding of L to high-concentration impurities in P, binding of P to P, and solvation of protons released upon L's binding to P).[6] An inherent source of inaccuracy in K_d determined by direct mass-spectrometry (MS) is a shift of equilibrium in Equation 1 during the transfer of L, P, and PL from the liquid or solid phase to the gas phase and during their ionization.[7] Accuracy of K_d determination with size-exclusion chromatography is affected by inevitable adsorption of L, P, and PL onto the stationary phase.[8] Finding K_d with Taylor dispersion assay requires fast re-equilibration and, hence, becomes inaccurate for stable PL; its accuracy is also affected by adsorption of L, P, and PL on the capillary wall.[9] Finally, affinity capillary electrophoresis suffers from the same inaccuracies as Taylor dispersion assay.[10] As a result of inherent inaccuracies, K_d values determined by different methods for the same PL may deviate by orders of magnitude. In some instances, K_d values differing by more than 100 times are considered consistent and kept in one data set.[11] Such large inaccuracies in K_d values lead to misinterpretation of experimental results, mistaken conclusions, and misconceptions. This alarming problem motivated our search for an approach for finding K_d of PL, that would be free of inherent sources of inaccuracy.

Fundamentally, finding K_d can be reduced to finding a fraction R of unbound L in the equilibrium mixture of L and P.[12] Finding R, in turn, requires fast separation (spectroscopic or physical) of L from PL. We hypothesized that a sought approach for determination of accurate K_d could be based on a deterministic phenomenon of transient incomplete separation (TIS) of solutes with different diffusion coefficients in a laminar pipe flow. TIS is a long-known phenomenon. It could be predicted as early as in 1910[13] and accurately modeled as early as in 1953.[14] TIS has been computer-simulated and experimentally studied in detail over the last four decades.[15] These studies provided important conceptual pillars and technical details for our work.

Let's start with explaining the concept of TIS in the context of our goal. TIS of species with largely different sizes, e.g. L and PL, occurs always when a short plug of their mixture is propagated within a laminar pipe flow (Figure 1a). Laminar pipe flow is established by a pressure difference between the capillary ends and has a characteristic parabolic profile of flow velocity.[16] The velocity is zero at the capillary walls and reaches its maximum in

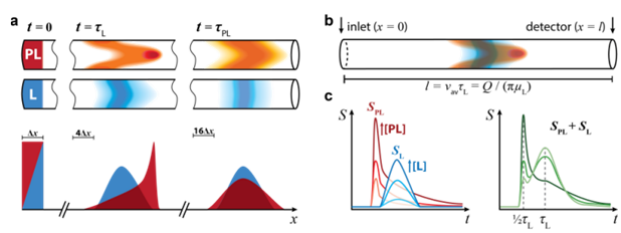

Figure 1. Concept of TIS of L (blue) from PL (red). **a)** TIS in space domain. Top: plugs of L and PL inside the capillary at three times: immediately after injection ($t = 0$), after propagation during a characteristic time of transverse diffusion of L ($\tau_L = a^2/\mu_L$), and after propagation during a characteristic time of transverse diffusion of PL ($\tau_{PL} = a^2/\mu_{PL}$), where a is a capillary inner radius and μ_L and μ_{PL} are diffusion coefficients of L and PL, respectively. Bottom: spatial profiles of average cross-sectional concentrations of L and PL at times $t = 0$, $t = \tau_L$, and $t = \tau_{PL}$; Δx refers to the initial plug length at $t = 0$. **b)** Detector positioned at distance $l = v_{av}\tau_L = Q/(\pi\mu_L) >> \Delta x$, were v_{av} is an average flow velocity and Q is a volumetric flow rate. **c)** TIS in time domain. Left: individual separagrams of L and PL at their increasing concentrations. Right: example of separagrams for three different values of R.

[*] Dr. N. Sisavath, Mr. J. L. Rukundo, Dr. V. A. Galievsky, Dr. J. Bao, Dr. S. Kochmann, Dr. A. S. Stasheuski, Prof. S. N. Krylov
Centre for Research on Biomolecular Interactions, York University, Toronto, Ontario M3J 1P3, Canada
E-mail: skrylov@yorku.ca
Homepage: http://www.yorku.ca/skrylov/
Dr. J. C. Yves Le Blanc
SCIEX, Concord, Ontario L4K 4V8, Canada
Supporting information including the Experimental Section and the ORCID identification numbers of the authors can be found under:

the capillary center. TIS of L from PL in the longitudinal direction is possible due to the difference in rates of transverse diffusion between small-size L and large-size PL. PL that is near the capillary center will diffuse to the capillary wall slower than L and, thus, will be displaced longitudinally by the flow more than L. PL located near the capillary wall will diffuse to the capillary center slower than L and will be displaced longitudinally by the flow less than L. As a result, during a short transitional stage (lasting a few seconds or less), a bulk of PL moves faster than a bulk of L, while a tail of PL moves slower than that of L. This separation is incomplete, *i.e.* the concentration profiles of L and PL do overlap.

We can now explain why and how TIS can serve as a foundation for measuring K_d of PL. Let's consider a schematic TIS system shown in Figure 1b, in which a capillary length (l) and a volumetric flow rate (Q) are linked with a diffusion coefficient of L (μ_L) as:

$$l/Q = 1/(\pi\mu_L) \quad (3)$$

Satisfying Equation 3 facilitate TIS of L from PL.[16] The equilibrium mixture is prepared by mixing P and L of total concentrations of $[P]_0$ and $[L]_0$, respectively, and incubating the mixture until reaction shown in Equation 1 approaches equilibrium. If a short plug of this mixture (sample plug) is subjected to TIS, concentration profiles of L and PL will be separated in the time domain as shown in Figure 1c, left. Further, let's assume that a signal can be measured for each of L and PL at the capillary exit and is proportional to the average cross-sectional concentration of each of them, $S_L \propto [L]$ and $S_{PL} \propto [PL]$. A cumulative signal S will then be a fractional superposition of individual signals (Figure 1c, right):

$$S = S_L R + S_{PL}(1-R) \quad (4)$$

where R is the above-mentioned fraction of free L ($R = [L]_{eq}/[L]_0$). Dependencies of the cumulative signal on time, $S(t)$, will be called "separagrams". We can see from Equation 4 that measuring S, S_L, and S_{PL} allows the determination of R:

$$R = (S - S_{PL})/(S_L - S_{PL}) \quad (5)$$

Finally, the knowledge of R allows finding K_d, e.g. through fitting an experimental dependence of R on $[P]_0$ (binding isotherm) with a theoretical one:[12]

$$R = -\frac{K_d + [P]_0 - [L]_0}{2[L]_0} + \sqrt{\left(\frac{K_d + [P]_0 - [L]_0}{2[L]_0}\right)^2 + \frac{K_d}{[L]_0}} \quad (6)$$

We see that TIS is theoretically suitable for measuring R and, thus, for finding K_d of PL. It is free of the earlier-discussed sources of inaccuracy present in other methods. Accordingly, we coin a name of "accurate constant via transient incomplete separation" (ACTIS) for this new approach of finding K_d.

A unique advantage of ACTIS is that TIS is based on processes, which are deterministic in nature. These processes can be accurately described by a system of equations for convection-diffusion and reversible binding reaction without any empirical coefficients (Section S1). As a result, ACTIS separagrams can be accurately computer-simulated, and performance of ACTIS, e.g. its accuracy, can be fully studied in-silico before any experimental proof-of-principle is attempted. ACTIS suitability for in-silico studies of its accuracy is very important as no experiment can be designed to prove the accuracy of K_d measurements because there is neither a reference-standard reaction with reference-standard K_d nor a reference-standard method for measuring K_d.

ACTIS is based on three key processes: 1) longitudinal advection of L, P, and PL in a laminar pipe flow, 2) their transverse diffusion, and 3) reversible binding of L and P. Longitudinal diffusion can be neglected.[17] We created a virtual ACTIS setup in COMSOL Multiphysics software and used this virtual setup to simulate separagrams under conditions similar to realistic ones in an envisioned proof-of-principle experiment. The diffusion coefficient of L (μ_L) is a key parameter in TIS as it defines the value of l/Q suitable for TIS of L from PL (see Equation 3). We

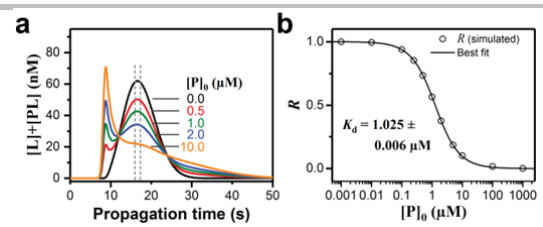

Figure 2. Determination of K_d by ACTIS using computer-simulated separagrams. **a)** Representative separagrams for $[L]_0 = 0.5$ μM, $[P]_0$ ranging from 0 to $10K_d$, rate constant of PL dissociation $k_{off} = 10^{-3}$ s^{-1}, rate constant of PL formation $k_{on} = 10^3$ M^{-1} s^{-1}, $K_d = k_{off}/k_{on} = 1$ μM, $\mu_L = 500$ μm^2/s, $\mu_P = \mu_{PL} = 50$ μm^2/s, inner capillary radius $a = 100$ μm, inlet-to-detector distance $l = 1$ cm, $Q = 1$ μL/min. The ordinate shows a sum of cross-sectional averages of [L] and [PL] in the detection window. **b)** A binding isotherm R versus $[P]_0$ (open circles), the best fit of the binding isotherm with Equation 6 (solid line), and the K_d value corresponding to the best fit.

used $\mu_L \approx 500$ μm^2/s for L of a size of small-molecule drug.[18] The values of l and Q in a virtual setup were 50 times smaller than in a real one to reduce computational time from hours to minutes. This reduction was possible due to scalability of these parameters and the results as long as Equation 3 is satisfied.[19] The remaining parameters (diffusion coefficients, rate constants, concentrations, and capillary radius) were set at realistic values.

Representative separagrams, simulated in a virtual experiment for constant $[L]_0$ and varying $[P]_0$, are shown in Figure 2a. Signals S, S_L, and S_{PL} required for determination of R with Equation 5 were obtained at time of the second-peak maximum. The found values of R were used to build a binding isotherm shown in Figure 2b. Non-linear regression was used to fit the isotherm with Equation 6 with K_d being a single fitting parameter. The K_d value that corresponded to the best fit differed from the one used in simulations by less than 3%. A small deviation from the ideal value was expected. Our virtual experiment included a number of non-idealities of a real experiment. For example, the initial sample plug after injection by a finite pressure had a finite length and a non-cylindrical shape. The limited number of points in the binding isotherm (akin to a real experiment) also contributes to the observed deviation. We then tested ACTIS for robustness to variations in μ_L, which may range from about 300 to 1500 μm^2/s for organic molecules with MW < 1 kDa.[20] Separagrams were simulated with l/Q ranging from $1/(3\pi\mu_L)$ to $3/(\pi\mu_L)$ (Figure S1) and found to be qualitatively similar to those obtained for $l/Q = 1/(\pi\mu_L)$ (Figure 2). The values of K_d were found not to deviate more than 5% from the value used in simulations, suggesting that a single value of l/Q can be used for different-size Ls. Thus, our study of ACTIS applied to simulated separagrams showed that ACTIS is both accurate and robust.

We then demonstrated a practical implementation of ACTIS, (see Section S2 for experimental details). A fluidic system capable of operating under conditions similar to those utilized in our virtual ACTIS setup was built. It was first coupled with a fluorescence detector and used to determine K_d of a non-covalent complex between bovine serum albumin (BSA) and fluorescein. Note that a fluorescence detector was used only to illustrate the suitability of different detectors for ACTIS and demonstrate that K_d found with ACTIS was not significantly affected by the choice of the detection mode if the detector could integrate the signal across the capillary. The obtained separagrams had a typical two-peak shape (Figure 3a) and were highly repeatable (Figure S2). Non-linear regression of the binding isotherm shown in Figure 3b with Equation 6 gave $K_d = 28 \pm 6$ μM. When reproduced on other days, the results for K_d varied within two folds (Figure S3).

We then coupled our ACTIS setup with an MS detector; we anticipate that MS will be the major mode of detection used with ACTIS. It is important to emphasize that ACTIS-MS is

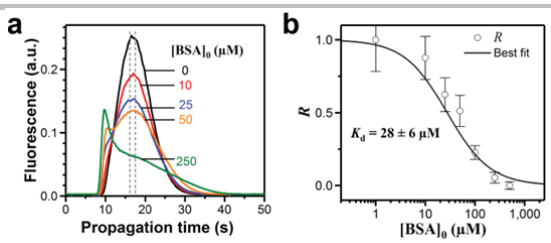

Figure 3. Determination of K_d by ACTIS with fluorescence detection. **a)** Representative separagrams for BSA–fluorescein complex from a set of separagrams obtained for $[\text{fluorescein}]_0 = 0.2$ μM and $[\text{BSA}]_0$ ranging from 0 to 0.5 mM. The vertical dashed lines show the time window at which an averaged signal was taken to calculate R with Equation 5. Experimental conditions were: internal capillary radius $a = 100$ μm, inlet-to-detector distance $l = 50$ cm, sample plug length = 3.2 cm, $Q = 50$ μL/min, 30 mM ammonium acetate buffer pH 7.5. **b)** A binding isotherm R versus $[\text{P}]_0$ (open circles, $n \geq 7$) and the best fit of the binding isotherm with Equation 6 (solid line). The uncertainty of R was obtained by error propagation (Section S4).

conceptually different from direct MS. Accuracy in direct MS suffers from a shift in the equilibrium between P, L, and PL during their transfer to the gas phase and ionization.[7] ACTIS-MS is immune to these effects since the information about R is built into the separagrams before sample transfer to the gas phase and ionization of L. To facilitate dissociation of PL during ionization, we utilized an atmospheric pressure chemical ionization source. ACTIS-MS was used to determine K_d for two protein-ligand complexes: BSA–fluorescein and alpha-1-acid glycoprotein (AGP)–alprenolol (Figure 4). The presence of P can either suppress or increase MS signal from L.[7, 21] We call this effect "masking", and we developed a signal-unmasking procedure to compensate for this effect (Section S3). The ACTIS-MS measurements revealed opposite masking effects for our two binding pairs; MS signal from fluorescein decreased with increasing $[\text{BSA}]_0$ (Figure 4a, left), while MS signal from alprenolol increased with increasing $[\text{AGP}]_0$ (Figure 4b, left). Separagrams were highly repeatable (Figures S4 and S5). We applied our signal-unmasking procedure to both sets of separagrams and obtained unmasked separagrams with a characteristic two-peak shape (Figures 4a,b, middle). Equation 5 was then used to build binding isotherms (Figures 4a,b, right). Note that the unmasking procedure is a simple mathematical operation that requires no additional experiments and can be automated. This compensation procedure has no effect in the absence of masking; therefore, it can be applied by default when MS detection is used for ACTIS. Finally, Equation 6 was used to fit the isotherms and find $K_d = 31 \pm 4$ μM for the BSA–fluorescein complex and $K_d = 1.4 \pm 0.2$ μM for the AGP–alprenolol complex. The largest deviation from these values obtained on different days did not exceed two folds (Figures S6 and S7). The K_d value for BSA–fluorescein obtained with ACTIS-MS is approximately two times higher than the value obtained by ACTIS with fluorescence detection. Our K_d values agree with the consensus literature values for both BSA–fluorescein (10–70 μM)[22] and AGP–alprenolol (2–35 μM)[23] complexes.

To conclude, in this proof-of-principle work, we introduce ACTIS as a generic approach for measuring accurate K_d of protein–small molecule complexes. While relying on separation, ACTIS does not require any form of stationary phase and does not impose any requirements on the protein or the small molecule except for having different sizes. ACTIS does not require immobilization of the protein or small molecule. TIS can be achieved even in a sub-second time scale, making ACTIS applicable to very unstable complexes. On the other hand, ACTIS is perfectly applicable to stable complexes. The upper level of K_d is limited by protein solubility and can be roughly defined as one tenth of the highest achievable protein concentration in a solution. The lower level of K_d is limited by the limit of detection for the ligand. For example, accurate determination of $K_d \approx 1$ nM (characteristic for high-affinity drugs) will require detecting 0.1 nM ligand with a signal to noise ratio of ≈ 100. Such sensitivity can be routinely achieved with fluorescence detection,[24] but remains a challenge with MS detection.[25]

As in other separation-based methods,[8,9] surface adsorption phenomena will distort separagrams and affect accuracy of K_d determined with ACTIS. However, time required for TIS is equal to the characteristic time of transverse diffusion of the ligand and much shorter than that of the protein and protein-ligand complex. Such a short separation time minimizes the extent of adsorption of the ligand and virtually prevents adsorption of the protein or the complex onto the inner capillary wall. Hence, we anticipate minor influence of surface adsorption phenomena on accuracy of ACTIS-measured K_d even if bare silica capillaries are used. Adsorption can be further minimized by passivating the capillary inner wall with an anti-adsorption layer. Advantageously, TIS should not be affected by such capillary modification if it does not introduce radius non-uniformity along the capillary.

While being free of inherent sources of inaccuracy, ACTIS is expectedly susceptible to errors associated with instrumentation, specifically, with detectors. For example, potential inability to uniformly integrate the signal through the entire capillary cross-section may lead to systematic errors. Therefore, optimally coupling the ACTIS fluidic system with different detectors will require further efforts of the engineering nature, which were not undertaken in this work. The observed two-fold difference in K_d found by ACTIS-fluorescence and ACTIS-MS is likely associated with the mentioned inaccuracies of cross-sectional signal integration. It can also be caused by the effect of residual salts, typically present in protein powder or stock solution, on MS signal from the ligand. The concentration of these residual salts gradually decreases with serial dilutions of the protein. The changing salt concentration can introduce a systematic error in R and, thus, in K_d. Instrument-independent errors in K_d can be caused by uncertainty

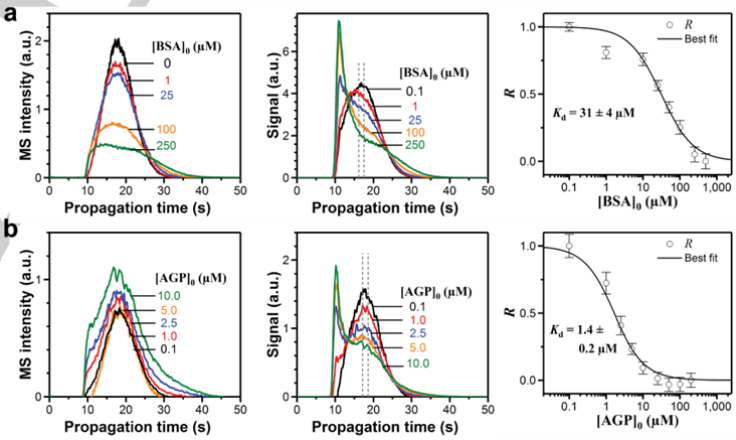

Figure 4. Determination of K_d by ACTIS with MS detection. **a)** Determination of K_d for the BSA–fluorescein complex; $[\text{fluorescein}]_0 = 0.2$ μM and $[\text{BSA}]_0$ ranges from 0 to 0.5 mM. MS signal for fluorescein was measured at $m/z = 287$. **b)** Determination of K_d for the AGP–alprenolol complex; $[\text{alprenolol}]_0 = 0.5$ μM and $[\text{AGP}]_0$ ranges from 0 to 0.2 mM. MS signal for alprenolol was measured at $m/z = 250$. Left: representative raw separagrams. Middle: separagrams after application of the signal-unmasking procedure; the vertical dashed lines show the time window at which an averaged signal was taken to calculate R with Equation 5. Right: binding isotherms R versus $[\text{P}]_0$ (open circles) and their best fits (solid lines) obtained with Equation 6. Conditions for ACTIS were similar to those described in the legend to Figure 3 except for $l = 100$ cm and $Q = 100$ μL/min (l/Q was the same). The uncertainty of R was obtained by error propagation (Section S4).

in protein concentration, e.g. due to 1) errors in its measurements, 2) adsorption on the walls during storage, or 3) its degradation. This uncertainty likely contributed to day-to-day variations in K_d values observed in our proof-of-principle experiments. Advantageously, ACTIS can be combined with any detection method which 1) can be coupled with a capillary, 2) uniformly integrates the signal through the capillary cross-section, 3) has sufficiently high signal readout speed, and 4) has a concentration limit of quantitation below K_d values of the studied complexes. A combination of ACTIS with MS appears to be the most suitable one for protein–small molecule complexes as it allows label-free detection of small molecules. However, due to matrix effects on ionization,[26] ACTIS-MS requires reasonably pure protein solutions. While TIS is not sensitive to buffer composition, MS is. Therefore, volatile buffers are preferable for ACTIS-MS over non-volatile. It has been previously shown that volatile buffers are suitable for studies of biomolecular interactions provided that they can support required pH and ionic strength.[27] If TIS is conducted in a non-volatile buffer, the sample should be diluted at the capillary exit with a sheath liquid suitable for both dissociation of the protein–ligand complex and efficient ionization of the ligand. In general, we foresee that most of future technical development of ACTIS will deal with its coupling with different detection systems and satisfying the four above-listed ACTIS requirement to detection systems.

Conflict of interest

The authors declare no conflict of interest.

Acknowledgements

This work was supported by the Natural Sciences and Engineering Research Council of Canada (grant number STPG-P 521331-2018) and Mitacs Canada (grant number IT08656).

Keywords: protein–small molecule complex • accurate equilibrium dissociation constant • transient incomplete separate • laminar pipe flow

[1] A. J. Firestone, J. K. Chen, *ACS Chem. Biol.* **2010**, *5*, 15–34.
[2] C. J. Zheng, L. Y. Han, C. W. Yap, Z. W Cao, Y. Z. Chen, *Pharmacol. Rev.* **2006**, *58*, 259–279.
[3] M. A. Cooper, *Nat. Rev. Drug Discov.* **2002**, *1*, 515–528 (2002).
[4] (a) C. J. Wienken, P. Baaske, U. Rothbauer, D. Braun, S. Duhr, *Nat. Commun.* **2010**, *1*, 100; (b) B. Lin, J. Qiu, J. Gerstenmeier, P. Li, H. Pien, J. Pepper, B. Cannningham, *Biosens. Bioelectron.* **2002**, *17*, 827–834.
[5] **(a)** A. Olaru, C. Bala, N. Jaffrezic-Renault, H. Y. Aboul-Enein, *Crit. Rev. Anal. Chem.* **2015**, *45*, 97–105; **(b)** P. Schuck, *Annu. Rev. Biophys. Biomol. Struct.* **1997**, *26*, 541–566. **(c)** H. Zhao, I. I. Gorshkova, G. L. Fu, P. Schuck, *Methods* **2013**, *59*, 328–335.
[6] S. Grüner, M. Neeb, L. J. Barandun, F. Sielaff, S. Kojima, T. Steinmetzer, F. Diederich, G. Klebe, *Biochim. Biophys. Acta* **2014**, *1840*, 2843–2850.
[7] E. N. Kitova, A. El-Hawiet, P. D. Schnier, J. S. Klassen, *J. Am. Soc. Mass. Spectrom.* **2012**, *23*, 431–441.
[8] J. F. Carpenter, T. W. Randolph, W. Jiskoot, D. J. Crommelin, C. R. Middaugh, G. Winter, *J. Pharm. Sci.* **2010**, *99*, 2200–2208.
[9] **(a)** S. M. Clark, L. Konermann, *Anal. Chem.* **2003**, *76*, 7077–7083; **(b)** H. Jensen, J. Østergaard, *J. Am. Chem. Soc.* **2010**, *132*, 4070–4071; **(c)** Bielejewska, A.; Bylina, A.; Duszczyk, K.; Fiałkowski, M.; Hołyst, R. *Anal. Chem.* **2010**, *82*, 5463–6469.
[10] **(a)** H. M. Albishri, S. El Deeb, N. AlGarabli, R. AlAstal, H. A. Alhazmi, M. Nachbar, D. A. El-Hady, H. Wätzig, *Bioanalysis* **2014**, *6*, 3369−3392. **(b)** M. Olabi, M. Stein, H. Wätzig, *Methods* **2018**, *146*, 76−92.
[11] H. Wätzig, I. Oltmann-Norden, F. Steinicke, H. A. Alhazmi, M. Nachbar, D. A. El-Hady, H. M. Albishri, K. Baumann, T. Exner, F. M. Böckler, S. El Deeb, *J. Comput.-Aided Mol. Des.* **2015**, *29*, 847–865.
[12] M. Kanoatov, V. A. Galievsky, S. M. Krylova, L. T. Cherney, H. K. Jankowski, S. N. Krylov, *Anal. Chem.* **2015**, *87*, 3099–3106.
[13] A. Griffiths, *Proc. Phys. Soc. London* **1910**, *23*, 190–197.
[14] G. I. Taylor, *Proc. R. Soc. A: Math. Phys. Eng. Sci.* **1953**, *219*, 186–203.
[15] **(a)** C. N. Trumbore, M. Grehlinger, M. Stowe, F. M. Keleher, *J. Chromatogr. A* **1985**, *322*, 443–454; **(b)** Ch.-H. Fischer, M. Giersig, *J. Chromatogr. A* **1994**, *688*, 97–105; **(c)** R. Umehara, H. Miyahara, A. Okino, M. Harada, T. Okada, *Anal. Sci.* **2012**, *28*, 359–365. (d) J. Chamieh, L. Leclercq, M. Martin, S. Slaoui, H. Jensen, J. Østergaard, H. Cottet, *Anal. Chem.* **2017**, *89*, 13487–13493.
[16] R. Umehara, M. Harada, T. Okada, *J. Sep. Sci.* **2009**, *32*, 472–478.
[17] V. Okhonin, E. Wong, S. N. Krylov, *Anal. Chem.* **2008**, *80*, 7482–7486.
[18] M. P. di Cagno, F. Clarelli, J. Våbenø, C. Lesley, S. D. Rahman, J. Cauzzo, E. Franceschinis, N. Realdon, P. C. Stein, *Mol. Pharmaceutics* **2018**, *15*, 1488–1494.
[19] **(a)** M. Harada, T. Kido, T. Masudo, T. Okada, *Anal. Sci.* **2005**, *21*, 491–496; **(b)** T. Okada, M. Harada, T. Kido, *Anal. Chem.* **2005**, *77*, 6041–6046.
[20] J. A. Schramke, S. F. Murphy, W. J. Doucette, W. D. Hintze, *Chemosphere* **1999**, *38*, 2381–2406.
[21] M. A. Sowole, S. Vuong, L. Konermann, *Anal. Chem.* **2015**, *87*, 9538–9545.
[22] **(a)** L.-O. Andersson, A. Rehnstrom, D. L. Eaker, *Eur. J. Biochem.* **1971**, *20*, 371–380; **(b)** C. W. Pinger, A. Castiaux, S. Speed, D. M. Spence, *J. Chem. Educ.* **2018**, *95*, 1662–1667; **(c)** M. S. Munson, J. M. Meacham, L. E. Locascio, D. Ross, *Anal. Chem.* **2008**, *80*, 172–178.
[23] **(a)** H. Imamura, T. Komori, A. Ismail, A. Suenaga, M. Otagiri, *Chirality* **2002**, *14*, 599–603; **(b)** J. Bao, S. M. Krylova, D. J. Wilson, O. Reinstein, P. E. Johnson, S. N. Krylov, *ChemBioChem* **2011**, *12*, 2551–2554; **(c)** P. A. McDonnel, G. W. Caldwell, J. A. Masucci, *Electrophoresis* **1998**, *19*, 448–454; **(d)** A. Yasgar, S, D. Furdas, D. J. Maloney, A. Jadhav, M. Jung, *PLoS One* **2012**, *7*, e45594.
[24] V. A. Galievsky, A. S. Stasheuski, S. N. Krylov, *Anal. Chim. Acta* **2016**, *935*, 58–81.
[25] W. F. Smyth, P. Brooks, *Electrophoresis* **2004**, *25*, 1413−1446.
[26] **(a)** A. Furey, M. Moriarty, V. Bane, B. Kinsella, M. Lehane, *Talanta* **2013**, *115*, 104−122; **(b)** L. l. Jessome, D. A. Volmer, *LCGC North Am.* **2006**, *24*, 498−510.
[27] J. Bao, S. N. Krylov, *Anal. Chem.* **2012**, *84*, 6944−6947.

Entry for the Table of Contents

Layout 2:

COMMUNICATION

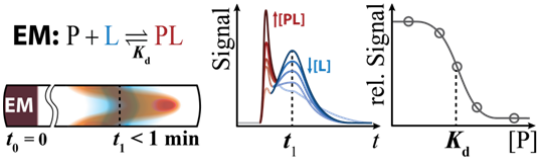

*Nicolas Sisavath, Jean Luc Rukundo, J. C. Yves Le Blanc, Victor A. Galievsky, Jiayin Bao, Sven Kochmann, Alexander S. Stasheuski and Sergey N. Krylov **

AAAA – BBBB

Protein–small molecule complex

We introduce "Accurate Constant via Transient Incomplete Separation" (ACTIS), an approach for measuring accurate equilibrium dissociation constant of protein–small molecule complexes.

ins

Table of Contents

Page

Section S1: Theoretical Background for Computer Simulation S2

Section S2: Experimental Details S4

Section S3: Quenching and Masking Effects in Signal Detection S7

Section S4: Error Propagation for *R* S8

Schematic S1 . . . . . S9

Schematic S2 . . . . . S9

Figure S1 . . . . . S10

Figure S2 . . . . . S11

Figure S3 . . . . . S12

Figure S4 . . . . . S13

Figure S5 . . . . . S14

Figure S6 . . . . . S15

Figure S7 . . . . . S16

This manuscript is accompanied by other supporting files:

COMSOL model (mph file)

Raw data and its evaluation for experiments (Excel files)

Digital data for figures (Origin files)

These files are also available in the preprint version of this manuscript at ChemRxiv (DOI: 10.26434/chemrxiv.7607078.v1).

Section S1: Theoretical Background for Computer Simulation

Separagrams were simulated with COMSOL in order to assess accuracy and robustness of ACTIS. In essence, the following set of partial differential equations describes the simulated processes of longitudinal advection, diffusion, and reversible-binding reaction of L and P forming complex PL:

$$\begin{aligned}
&\frac{\partial[\mathrm{P}]}{\partial t}+v(r)\frac{\partial[\mathrm{P}]}{\partial x}-\mu_{\mathrm{P}}\left(\frac{\partial^2[\mathrm{P}]}{\partial^2 x}+\frac{1}{r}\frac{\partial}{dr}\left(r\frac{\partial[\mathrm{P}]}{dr}\right)\right)=-k_{\mathrm{on}}[\mathrm{P}][\mathrm{L}]+k_{\mathrm{off}}[\mathrm{PL}]\\
&\frac{\partial[\mathrm{L}]}{\partial t}+v(r)\frac{\partial[\mathrm{L}]}{\partial x}-\mu_{\mathrm{L}}\left(\frac{\partial^2[\mathrm{L}]}{\partial^2 x}+\frac{1}{r}\frac{\partial}{dr}\left(r\frac{\partial[\mathrm{L}]}{dr}\right)\right)=-k_{\mathrm{on}}[\mathrm{P}][\mathrm{L}]+k_{\mathrm{off}}[\mathrm{PL}]\\
&\frac{\partial[\mathrm{PL}]}{\partial t}+v(r)\frac{\partial[\mathrm{PL}]}{\partial x}-\mu_{\mathrm{PL}}\left(\frac{\partial^2[\mathrm{PL}]}{\partial^2 x}+\frac{1}{r}\frac{\partial}{dr}\left(r\frac{\partial[\mathrm{PL}]}{dr}\right)\right)=k_{\mathrm{on}}[\mathrm{P}][\mathrm{L}]-k_{\mathrm{off}}[\mathrm{PL}]
\end{aligned} \tag{S1}$$

where t is time, x is longitudinal distance from the capillary inlet, r is radial distance from the capillary center, μ_{P}, μ_{L}, and μ_{PL} are diffusion coefficients of P, L, and PL, respectively, k_{on} and k_{off} are rate constants of the reversible binding reaction:

$$\mathrm{P}+\mathrm{L}\underset{k_{\mathrm{off}}}{\overset{k_{\mathrm{on}}}{\rightleftharpoons}}\mathrm{PL} \tag{S2}$$

and $v(r)$ is the parabolic velocity profile of laminar pipe flow (Hagen–Poiseuille flow) described by:

$$v(r)=v_{\max}\left(1-\frac{r^2}{a^2}\right),\quad v_{\max}=2v_{\mathrm{av}} \tag{S3}$$

where a is a capillary inner radius, $v_{\max}$ is the velocity in the capillary center ($r = 0$), and v_{av} is the average flow velocity, which can be expressed through the volumetric flow rate Q_v:

$$v_{\mathrm{av}}=\frac{Q_v}{\pi a^2} \tag{S4}$$

with:

$$\begin{aligned}
&Q_v = Q_{\mathrm{transfer}},\ 0 \le t < t_{\mathrm{transfer}}\\
&Q_v = Q >> Q_{\mathrm{transfer}},\ t_{\mathrm{transfer}} \le t
\end{aligned} \tag{S5}$$

where Q_{transfer} is the flow rate of sample-plug transfer into the separation capillary during the corresponding transfer time, t_{transfer}; Q is the flow rate of sample propagation through the separation capillary (TIS flow rate).

The initial conditions for space inside the capillary are:

$$[\mathrm{P}]=0,\quad [\mathrm{L}]=0,\quad [\mathrm{PL}]=0;\quad 0\le x\le l,\quad t=0 \tag{S6}$$

where l is the length of the capillary. The time-dependent boundary conditions are:

$$\begin{aligned}
&[\mathrm{P}]=[\mathrm{P}]_{\mathrm{eq}},\ [\mathrm{L}]=[\mathrm{L}]_{\mathrm{eq}},\ [\mathrm{PL}]=[\mathrm{PL}]_{\mathrm{eq}};\ x=0,\ 0\le t<\tfrac{1}{2}t_{\mathrm{transfer}},\ Q_v=Q_{\mathrm{transfer}}\\
&[\mathrm{P}]=0,\ [\mathrm{L}]=0,\ [\mathrm{PL}]=0;\ x=0,\ \tfrac{1}{2}t_{\mathrm{transfer}}\le t<t_{\mathrm{transfer}},\ Q_v=Q_{\mathrm{transfer}}\\
&[\mathrm{P}]=0,\ [\mathrm{L}]=0,\ [\mathrm{PL}]=0;\ x=0,\ t_{\mathrm{transfer}}\le t,\ Q_v=Q
\end{aligned} \tag{S7}$$

where the second line corresponds to injection of a water plug into the capillary to slowly displace the sample-plug from the capillary inlet. Time-independent boundary conditions are:

$$\begin{aligned} &\partial_r[\mathrm{P}]=0, \quad \partial_r[\mathrm{L}]=0, \quad \partial_r[\mathrm{PL}]=0; \quad r=a \\ &\partial_x[\mathrm{P}]=0, \quad \partial_x[\mathrm{L}]=0, \quad \partial_x[\mathrm{PL}]=0; \quad x=l \end{aligned} \tag{S8}$$

The injected equilibrium mixture contained L, P, and PL at equilibrium concentrations of $[\mathrm{L}]_{\mathrm{eq}}$, $[\mathrm{P}]_{\mathrm{eq}}$, and $[\mathrm{PL}]_{\mathrm{eq}}$, respectively:

$$[\mathrm{L}]_{\mathrm{eq}} = [\mathrm{L}]_0 - [\mathrm{PL}]_{\mathrm{eq}} \tag{S9}$$

$$[\mathrm{L}]_{\mathrm{eq}} = \frac{-([\mathrm{P}]_0 - [\mathrm{L}]_0 + K_{\mathrm{d}}) + \sqrt{([\mathrm{L}]_0 - [\mathrm{P}]_0 + K_{\mathrm{d}})^2 + 4[\mathrm{P}]_0 K_{\mathrm{d}}}}{2} \tag{S10}$$

$$[\mathrm{PL}]_{\mathrm{eq}} = \frac{([\mathrm{L}]_0 + [\mathrm{P}]_0 + K_{\mathrm{d}}) - \sqrt{([\mathrm{L}]_0 - [\mathrm{P}]_0 + K_{\mathrm{d}})^2 + 4[\mathrm{P}]_0 K_{\mathrm{d}}}}{2} \tag{S11}$$

$$[\mathrm{P}]_{\mathrm{eq}} = [\mathrm{P}]_0 - [\mathrm{PL}]_{\mathrm{eq}} \tag{S12}$$

where $[\mathrm{L}]_0$ and $[\mathrm{P}]_0$ are initial concentrations of L and P, respectively. Transformations of reactive species inside capillary were described with reaction rates $\mathrm{Rate}_{\mathrm{L}}$, $\mathrm{Rate}_{\mathrm{P}}$, and $\mathrm{Rate}_{\mathrm{PL}}$:

$$\mathrm{Rate}_{\mathrm{L}} = -k_{\mathrm{on}}[\mathrm{P}][\mathrm{L}] + k_{\mathrm{off}}[\mathrm{PL}] \tag{S13}$$

$$\mathrm{Rate}_{\mathrm{P}} = -k_{\mathrm{on}}[\mathrm{P}][\mathrm{L}] + k_{\mathrm{off}}[\mathrm{PL}] \tag{S14}$$

$$\mathrm{Rate}_{\mathrm{PL}} = k_{\mathrm{on}}[\mathrm{P}][\mathrm{L}] - k_{\mathrm{off}}[\mathrm{PL}] \tag{S15}$$

Section S2: Experimental Details

General. All chemicals and buffer components were purchased from Sigma-Aldrich (Oakville, ON, Canada). Fused-silica capillaries were purchased from Molex (Polymicro Technologies, Phoenix, AZ, USA). All measurements were carried out at room temperature (22 ± 2 °C). A single buffer, 30 mM ammonium acetate pH 7.5, was utilized to prepare all solutions, accordingly, when we refer to the buffer, we imply 30 mM ammonium acetate pH 7.5.

Simulation of separagrams. To simulate separagrams we used COMSOL Multiphysics software, version 5.3, with the "Transport of Diluted Species" module, which incorporates mass transfer equations (the model is available in the Supporting files). The respective system of differential equations with initial and boundary conditions are shown in Section S1. The laminar flow can be obtained if the Reynolds number, $\mathrm{Re} \equiv 2Q/(\nu_k \pi a)$, is less than a thousand, where Q is the volumetric flow rate, ν_k is the kinematic viscosity of a liquid, and a is the capillary inner radius. As a result, water ($\nu_k \approx 10^{-6}$ m^2/s) will have laminar flow in a narrow capillary (e.g. $a \approx 100$ μm) as long as $Q \leq 1$ mL/min. The simulation parameters were chosen to ensure that the flow was laminar.

The simulation parameters were also chosen in order to have the detection time of the peak of L corresponding to the characteristic diffusion time of L, $\tau_L = a^2/\mu_L$. This condition resulted in the following ratio: $l/Q \approx 1/(\pi\mu_L)$. Considering L with $\mu_L = 500$ μm^2/s, and a capillary with an inner radius of $a = 100$ μm, the detection time would be 20 s, which is a reasonable value for the prototype experimental setup. Computational time depends on the dimensions of the simulated capillary. Thus, to reduce this time, the inlet-to-detector distance l can be scaled down while the ratio l/Q is kept constant. $l = 1$ cm and detection window of 0.1 mm were chosen which resulted in the TIS flow rate of $Q \approx 0.9$ μL/min and for simplicity $Q = 1$ μL/min was used. Sample plug injection flow rate should be smaller than TIS flow rate. Thus, sample-plug injection was done with a flow rate of 0.1 μL/min during 12 s resulting in a plug of approximately 0.6 mm in length. Subsequently, a water plug was injected into the capillary with 0.1 μL/min during 12 s to slowly displace the sample-plug from the capillary inlet (plug end distance from the capillary inlet was approximately 0.6 mm). The rest of simulation parameters were as follows: $k_{off} = 10^{-3}$ s^{-1}, $k_{on} = 10^3$ M^{-1}s^{-1} ($K_d = k_{off}/k_{on} = 1$ μM), $\mu_P = \mu_{PL} = 50$ μm^2/s, $[L]_0 = 0.5$ μM, temperature = 293.15 K (used by COMSOL to define physical parameters of water, e.g. viscosity and density). $[P]_0$ was varied from 1 nM to 1 mM using 11 different concentrations plus a run at $[P]_0 = 0$. Further, to study robustness of ACTIS to variations in μ_L we simulated separagrams with l/Q ranging from $1/(3\pi\mu_L)$ to $3/(\pi\mu_L)$ by varying l (Figure S1).

Since the plug shape is symmetric with respect to the capillary longitudinal axis, the capillary was modeled with a 2D axisymmetric shape to further reduce the computation time. The virtual detector was placed at the end of the virtual capillary. The modeled shape of the capillary was divided into a rectangular mesh with a density of 5000 cells (20 × 250, radial and axial meshes, respectively) per centimeter. The detection zone for each l (1, 1/3, 1/2, 2 and 3 cm) was 0.1-mm-long and was also divided into a rectangular mesh but with 200 cells (20 × 10, radial and axial meshes, respectively). The Iterative Generalized Minimal Residual (GMRES) solver was used in COMSOL to approximate concentrations of reactive species in a time-dependent manner over the defined mesh. The output signal was defined as a sum of individually averaged concentrations of L and PL inside the 200-cell detection zone.

ACTIS fluidic setup. A general schematic of the ACTIS fluidic setup is shown in Schematic S1, and a more detailed schematic — emphasizing valve operation during the measurement cycle — is shown in Schematic S2. Custom software written in LabVIEW was utilized to control the valves through a PCI-6035E board (National Instruments, Austin, TX, USA).

Buffer and sample solutions were injected by NE-300 syringe pumps (New Era Pump Systems Inc., Farmingdale, NY, USA) utilizing syringes of 10 mL and 1 mL, respectively (Becton, Dickinson and Company; Mississauga, ON, Canada). While being identical, these pumps had different functions and were named the "sample pump" and the low pressure pump (LPP) for sample loading and sample transfer, respectively. The sample plug was propagated through the separation capillary by a high pressure pump (HPP) from a solvent delivery module of System Gold HPLC 128NM (Beckman Coulter,

Fullerton, CA, USA) for fluorescence measurements and by HPP from Nexera SR System HPLC module (Shimadzu Scientific Instruments, MD, USA) for MS measurements. Two dual-position valves (Rheodyne MXP7900-000 from IDEX Health & Science, Oak Harbor, WA, USA) were used to switch flow pathways in the fluidic setup. The sample syringe was connected to Valve 1 with a 30-cm long uncoated fused-silica capillary of 150-µm inner diameter and 360-µm outer diameter (through capillary tubing fittings from IDEX Health & Science); this capillary was pre-filled with the sample before the Sample loading stage (see below). The buffer syringe was connected to the valves using a polyethylene tubing of 1.57-mm inner diameter and 2.08-mm outer diameter (BD Intramedic, purchased from Fisher Scientific, Ottawa, ON, Canada). An uncoated fused-silica capillary of 75-µm inner diameter, 360-µm outer diameter, and 22.7-cm length was utilized as an injection loop with a volume of $V_{loop} = 1$ µL. The injection loop was placed between Valves 1 and 2. An additional mock loop identical to the injection loop was positioned between Valves 1 and 2. An uncoated fused-silica capillary of 200-µm inner diameter and 360-µm outer diameter was used for TIS and is named "separation capillary"; it was connected to Valve 2. The total length of the capillary was 60 cm (inlet-to-detector distance was $l = 50$ cm) for a setup with fluorescence detection and 100 cm (inlet-to-detector distance was $l = 100$ cm) for a setup with MS detection. Two mock capillaries identical to the separation capillary were connected to Valve 2. The mock loop and the mock capillaries were used to allow the continuous operation of LPP and HPP and ensure that they ran under constant back-pressures.

The pumps operated at the following flow rates: the sample pump at 15 µL/min, LPP at 5 µL/min, HPP for fluorescence detection at $Q = 50$ µL/min and HPP for MS detection at $Q = 100$ µL/min (to keep l/Q = const = 1 cm min µL^{-1}). An 86-s-long measurement cycle included 3 stages. Switching between the stages was done by changing positions of the valves during less than 0.1 s. For the very first run and cycle, the sample was pre-filled into the capillary connecting the sample pump and Valve 1 (using its position II) before starting the cycle; in subsequent runs and cycles, this pre-filling was done during the third stage.

The first stage was 12-s-long sample loading into the 1-µL injection loop (Schematic S2a). Valves 1 and 2 were in position I. The sample pump moved sample volume equal to $3 \times V_{loop}$ through the injection loop to insure its complete filling. LPP was pumping the buffer through the mock loop and mock capillary. HPP was pumping the buffer through the separation capillary.

The second stage was 24-s-long sample transfer from the injection loop into the separation capillary (Schematic S2b). Both valves were in position II. LPP moved the buffer *via* the sample-containing injection loop. The sample was subsequently transferred into the separation capillary. At the end of this stage a sample plug of approximately 3.2 cm in length was 3.2 cm away from the inlet of the separation capillary. HPP was pumping the buffer through the mock capillary. The sample pump was idle.

The third stage was 50-s-long sample propagation through the separation capillary (Schematic S2c). Valve 2 was in position I, while Valve 1 stayed in position II. The sample pump was used for pre-filling. HPP pumped the buffer into the separation capillary for TIS of PL from L. LPP was pumping the buffer through the injection loop. In total the injection loop was rinsed with $6 \times V_{loop}$ ($2 \times V_{loop}$ during the second stage and $\approx 4 \times V_{loop}$ during the third stage).

Fluorescence detector. A diode-pumped solid state laser (AixiZ, Houston, TX, USA) was a light source for excitation of fluorescence. The laser beam had a diameter of about 2 mm and a power of 60 mW at 473 nm. Two subsequent neutral filters of 0.4 and 1.0 optical density (NE04B and NE10B, Thorlabs, Newton, NJ, USA) were used to attenuate laser power to ≈ 2 mW. Fluorescence emission was collected by an MPlan 60× objective lens (NA = 0.7 at 90°) with an additional optical bandpass filter of 525 ± 25 nm (Semrock, Rochester, NY, USA). A photocathode of the photomultiplier tube R1477 (Hamamatsu Photonics, Hamamatsu, Japan) was biased at –400 V. A 20 Hz low-pass electronic filter was introduced between the photomultiplier tube and the analog-to-digital signal converter PCI-6035E (National Instruments, Austin, TX, USA), to reduce electronic noise. Fluorescence data collection was controlled with the same custom LabVIEW software that was used to control the valves in the fluidic setup.

Fluorescence-based determination of K_d for the fluorescein-BSA complex. Concentration of fluorescein was 0.2 μM. Concentration of BSA ranged from 0.1 μM to 1 mM. The buffer was 30 mM ammonium acetate pH 7.5. Fluorescein-BSA mixtures were vortexed and incubated at room temperature for ≈ 2 h to establish equilibrium in the reversible binding reaction. After the incubation, the EMs were subjected to ACTIS as described in the "ACTIS fluidic setup" section. To obtain R for each BSA concentration the experiment was repeated at least 5 times. The value of K_d was obtained by fitting R versus $[P]_0$ with their theoretical dependence as described in the "Data acquisition and treatment" section.

MS detector. The output of the separation capillary was inserted into the MS ionization source (Turbo V ion source with APCI probe, AB Sciex, Vaughan, ON, Canada); APCI was selected as it is less prone to ion suppression than e.g. electrospray ionization (ESI). MS detection was done with a QTRAP 6500+ instrument (AB Sciex, Vaughan, ON, Canada). The optimal acceleration and focusing conditions were achieved by using a 60-V declustering potential at 525 ºC and 90-psi gas pressure. The MS analyses were performed in positive mode, and the analyzed small molecules – fluorescein and alprenolol – were detected at m/z of 287 and 250, respectively. The m/z signals were processed using Analyst QS 2.0 software. MS data collection was controlled with the same custom LabVIEW software and PCI-6035E board that were used to control the valves in the fluidic setup.

Determination of K_d for fluorescein-BSA and alprenolol-AGP complexes by ACTIS with MS detection. The experiments were performed to measure K_d of complexes between BSA (0.1–500 μM) and fluorescein (0.2 μM) as well as between AGP (0.1–500 μM) and alprenolol (0.5 μM). The buffer was 30 mM ammonium acetate pH 7.5. BSA-fluorescein and AGP–alprenolol mixtures were incubated at room temperature for ≈ 2 h to establish equilibrium in the reversible binding reaction. After incubation, the EMs were subjected to ACTIS as described in the "ACTIS fluidic setup" section. Measurements of R for each protein concentration were done in triplicates. K_d was obtained by fitting R versus $[P]_0$ with their theoretical dependence as described in the "Data acquisition and treatment" section.

Data acquisition and treatment. The experimental data acquisition was triggered at the beginning of the sample-transfer stage (second stage); this mimicked the way of treatment of simulated separagrams. The acquired or simulated data were evaluated using Excel and OriginPro. For each experimental signal of the MS data the background taken at the beginning of the recorded separagram ($t < 5$ s) was subtracted; the background of the fluorescence data was already within the limits of signal noise and, hence, was not subtracted. The following equation was used to approximate R in Equation 5 in the main text:

$$R \approx \frac{S_{[P]_0} - S_{[P]_0 >> K_d}}{S_{[P]_0 << K_d} - S_{[P]_0 >> K_d}} \tag{S16}$$

where $S_{[P]_0}$ is a signal at the intermediate value of $[P]_0$. Here and in the following, we approximate S_{PL} with $S_{[P]_0 \gg Kd}$, S_L with $S_{[P]_0 \ll Kd}$. The main reason for such approximation is that strictly speaking S_{PL} corresponds to $[PL] = [L]_0$ which cannot be achieved in a real experiment since it requires $[P] \to \infty$. Therefore S_{PL} is approximated with $S_{[P]_0 \gg Kd}$, and, symmetrically, S_L is approximated with $S_{[P]_0 \ll Kd}$. Signals required for determination of R were obtained by averaging points within a time-window near $\tau_L = 20$ s. The middle of the window corresponded exactly to the maximum of the second peak (e.g. 16.63 s in Figure 2a) taken from the separagram of the smallest $[P]_0 \neq 0$. The first point and the last point of the window corresponded exactly to 0.96 and 1.04 of the position of this maximum of the second peak, respectively (e.g. 15.97 s and 17.30 s in Figure 2a). This window width was chosen to increase the signal-to-noise ratio while covering only the tip of the peak; for our data, the window width ranged between 1.2 and 1.5 s. The averaged signal at each concentration of sample was measured/simulated $n \geq 3$ times. The standard deviation (σ) for each R was obtained by simple error propagation based on Equation S16 (Section S4). K_d was obtained by fitting the dependence of R on $[P]_0$ with Equation 6 in the main text. A weighted non-linear fitting was performed using the Levenberg-Marquardt algorithm; each point had a weight of σ^{-2}.

Section S3: Quenching and Masking Effects in Signal Detection

In our above-described *in-silico* study of ACTIS, we used a direct link between the signal and a cumulative concentration of L and PL: $S = [L] + [PL]$. In reality, the signals from L and PL depend on the nature of both P and L as well as the mode of detection. P can influence the signal from L by binding L (we'll call this influence "quenching") and by being in the detector at the time of registration (we'll call this influence "masking").

If optical (e.g. fluorescence) detection is used, static quenching with a constant quenching coefficient is likely to be present. On the other hand, masking (i.e. dynamic quenching) in optical detection is unlikely. As a result, the signal in optical detection is multiplied with a constant quenching coefficient. Therefore, the signal will satisfy the requirement of signal superposition expressed by Equation 4. Thus, while static quenching will affect separagrams, its presence will not affect the K_d value determined with the ACTIS procedure illustrated in Figure 2.

If MS is used for detection of L, conditions should be created to dissociate PL during ionization so that detection of the intact PL is not required. The dissociation of PL will automatically exclude signal quenching. However, the presence of unbound P can affect ionization of unbound L and, in turn, signal from L,[1] causing its masking (either increase or decrease in the signal). To "unmask" the signal, an operator $\hat{O}$, which describes a mathematical compensation procedure, should be applied to the raw MS signal $S_{raw}(t)$:

$$S(t) = \hat{O} S_{raw}(t) \tag{S17}$$

Subsequently, this "unmasked" signal can be used for K_d determination using the standard ACTIS protocol.

A simple masking-compensation procedure can be built upon two facts. First, P and PL have similar separagrams; these separagrams can be robustly and accurately computer-simulated. Second, the concentration (and amount) of L is constant in experiments with varying $[P]_0$; thus, the areas under the separagrams should be constant. Based on these two facts, we suggest a compensation procedure with two operations: 1) multiplication (operator $\hat{O}_M$) of the measured separagrams by the simulated profile of P and 2) subsequent normalization (operator $\hat{O}_N$) of the separagrams to make the areas (integrals) under them equal to the area (integral) under the experimental separagram of L corresponding to the smallest amounts of protein ($[P]_0 << K_d$):

$$\hat{O} \equiv \hat{O}_N \hat{O}_M, \quad \hat{O}_M = \tilde{S}_P(t), \quad \hat{O}_N = \frac{\int \tilde{S}_P(t) S_{[P]_0 << K_d}(t) dt}{\int \tilde{S}_P(t) S_{raw}(t) dt} \tag{S18}$$

where $\tilde{S}_P$ is the dimensionless simulated separagram of pure P. $\hat{O}_N$ can be greater or smaller than unity, i.e. the presence of P can either suppress or enhance ionization of L. Combining Equations S17 with Equation S18 provides an instruction on how to process the raw signal in order to get the unmasked signal for K_d determination:

$$S(t) = \frac{\int \tilde{S}_P(t) S_{[P]_0 << K_d}(t) dt}{\int \tilde{S}_P(t) S_{raw}(t) dt} \tilde{S}_P(t) S_{raw}(t) \tag{S19}$$

This unmasked signal can be used in Equation S16 to find R and determine K_d.

The described compensation procedure limits the compensated effect of P on the signal from L to the linear term: masking is proportional to the concentration of P if the buffer composition is kept constant in serial dilutions of the stock solution of the protein. While higher-order effects are theoretically possible, they are assumed to have lower weights than the linear effect. This compensation procedure has no effect in the absence of masking; therefore, it can be applied by default when MS detection is used for ACTIS.

[1] (a) E. N. Kitova, A. El-Hawiet, P. D. Schnier, J. S. Klassen, *J. Am. Soc. Mass. Spectrom.* **2012**, *23*, 431−441;
(b) M.A. Sowole, S. Vuong, L. Konermann, *Anal. Chem.* **2015**, *87*, 9538−9545.

Section S4: Error Propagation for *R*

Equation S16 is used to obtain uncertainty of R through error propagation. The uncertainty of R expressed by the standard deviation (SD), $\sigma(R)$, can be obtained as following:

$$\sigma(R) \approx \sqrt{\left(\frac{\partial R}{\partial S_{[\mathrm{P}]_0}}\sigma(S_{[\mathrm{P}]_0})\right)^2 + \left(\frac{\partial R}{\partial S_{[\mathrm{P}]_0 \gg K_\mathrm{d}}}\sigma(S_{[\mathrm{P}]_0 \gg K_\mathrm{d}})\right)^2 + \left(\frac{\partial R}{\partial S_{[\mathrm{P}]_0 \ll K_\mathrm{d}}}\sigma(S_{[\mathrm{P}]_0 \ll K_\mathrm{d}})\right)^2} \tag{S20}$$

where $\sigma(X)$ is the standard deviation of X. Partial derivatives can be calculated using average values S^{AV}.

$$\frac{\partial R}{\partial S_{[\mathrm{P}]_0}} = \frac{1}{S^{\mathrm{AV}}_{[\mathrm{P}]_0 \ll K_\mathrm{d}} - S^{\mathrm{AV}}_{[\mathrm{P}]_0 \gg K_\mathrm{d}}} \tag{S21}$$

$$\frac{\partial R}{\partial S_{[\mathrm{P}]_0 \gg K_\mathrm{d}}} = \frac{-S^{\mathrm{AV}}_{[\mathrm{P}]_0 \ll K_\mathrm{d}} + S^{\mathrm{AV}}_{[\mathrm{P}]_0 \gg K_\mathrm{d}} + S^{\mathrm{AV}}_{[\mathrm{P}]_0} - S^{\mathrm{AV}}_{[\mathrm{P}]_0 \gg K_\mathrm{d}}}{(S^{\mathrm{AV}}_{[\mathrm{P}]_0 \ll K_\mathrm{d}} - S^{\mathrm{AV}}_{[\mathrm{P}]_0 \gg K_\mathrm{d}})^2} = \frac{S^{\mathrm{AV}}_{[\mathrm{P}]_0} - S^{\mathrm{AV}}_{[\mathrm{P}]_0 \ll K_\mathrm{d}}}{(S^{\mathrm{AV}}_{[\mathrm{P}]_0 \ll K_\mathrm{d}} - S^{\mathrm{AV}}_{[\mathrm{P}]_0 \gg K_\mathrm{d}})^2} \tag{S22}$$

$$\frac{\partial R}{\partial S_{[\mathrm{P}]_0 \ll K_\mathrm{d}}} = \frac{-(S^{\mathrm{AV}}_{[\mathrm{P}]_0} - S^{\mathrm{AV}}_{[\mathrm{P}]_0 \gg K_\mathrm{d}})}{(S^{\mathrm{AV}}_{[\mathrm{P}]_0 \ll K_\mathrm{d}} - S^{\mathrm{AV}}_{[\mathrm{P}]_0 \gg K_\mathrm{d}})^2} = \frac{S^{\mathrm{AV}}_{[\mathrm{P}]_0 \gg K_\mathrm{d}} - S^{\mathrm{AV}}_{[\mathrm{P}]_0}}{(S^{\mathrm{AV}}_{[\mathrm{P}]_0 \ll K_\mathrm{d}} - S^{\mathrm{AV}}_{[\mathrm{P}]_0 \gg K_\mathrm{d}})^2} \tag{S23}$$

As a result, σR can be written as following:

$$\sigma(R) \approx \frac{1}{S^{\mathrm{AV}}_{[\mathrm{P}]_0 \ll K_\mathrm{d}} - S^{\mathrm{AV}}_{[\mathrm{P}]_0 \gg K_\mathrm{d}}} \sqrt{\begin{array}{l}\left(\sigma(S_{[\mathrm{P}]_0})\right)^2 + \left(\dfrac{S^{\mathrm{AV}}_{[\mathrm{P}]_0} - S^{\mathrm{AV}}_{[\mathrm{P}]_0 \ll K_\mathrm{d}}}{S^{\mathrm{AV}}_{[\mathrm{P}]_0 \ll K_\mathrm{d}} - S^{\mathrm{AV}}_{[\mathrm{P}]_0 \gg K_\mathrm{d}}}\sigma(S_{[\mathrm{P}]_0 \gg K_\mathrm{d}})\right)^2 + \\ \left(\dfrac{S^{\mathrm{AV}}_{[\mathrm{P}]_0 \gg K_\mathrm{d}} - S^{\mathrm{AV}}_{[\mathrm{P}]_0}}{S^{\mathrm{AV}}_{[\mathrm{P}]_0 \ll K_\mathrm{d}} - S^{\mathrm{AV}}_{[\mathrm{P}]_0 \gg K_\mathrm{d}}}\sigma(S_{[\mathrm{P}]_0 \ll K_\mathrm{d}})\right)^2\end{array}} \tag{S24}$$

In case of MS data, values from unmasked signals are substituted in Equation S16. Thus, Equation S24 should be modified to take into account the signal correction (unmasking) procedure. The uncertainty $\sigma(S(t))$ at a specific time t for the unmasked MS signals S_{raw} should be calculated using Equation S19 as follows:

$$\sigma(S(t)) = \sigma\left(\frac{\int \tilde{S}_\mathrm{P}(t) S_{[\mathrm{P}]_0 << K_\mathrm{d}}(t)dt}{\int \tilde{S}_\mathrm{P}(t) S_{\mathrm{raw}}(t)dt}\tilde{S}_\mathrm{P}(t) S_{\mathrm{raw}}(t)\right) \tag{S25}$$

Due to good repeatability of the separagrams (Figures S2, S4, and S5) the areas under the individual separagrams can be substituted with the areas of the averaged separagrams, and Equation S25 can be modified as follows:

$$\begin{aligned}\sigma(S(t)) &= \sigma\left(\frac{\int \tilde{S}_\mathrm{P}(t) S_{[\mathrm{P}]_0 << K_\mathrm{d}}(t)dt}{\int \tilde{S}_\mathrm{P}(t) S_{\mathrm{raw}}(t)dt}\tilde{S}_\mathrm{P}(t) S_{\mathrm{raw}}(t)\right) \approx \sigma\left(\frac{\int \tilde{S}_\mathrm{P}(t) S^{\mathrm{AV}}_{[\mathrm{P}]_0 << K_\mathrm{d}}(t)dt}{\int \tilde{S}_\mathrm{P}(t) S^{\mathrm{AV}}_{\mathrm{raw}}(t)dt}\tilde{S}_\mathrm{P}(t) S_{\mathrm{raw}}(t)\right) \approx \\ &\approx \frac{\int \tilde{S}_\mathrm{P}(t) S^{\mathrm{AV}}_{[\mathrm{P}]_0 << K_\mathrm{d}}(t)dt}{\int \tilde{S}_\mathrm{P}(t) S^{\mathrm{AV}}_{\mathrm{raw}}(t)dt}\tilde{S}_\mathrm{P}(t)\sigma(S_{\mathrm{raw}}(t))\end{aligned} \tag{S26}$$

where $\sigma(S_{\mathrm{raw}}(t))$ is the SD of the MS values taken at time t from the raw MS signal. Thus, $\sigma(S(t))$ were calculated using Equation S26 and then were substituted in Equation S24 to obtain $\sigma(R)$ necessary to assess the uncertainty of K_d.

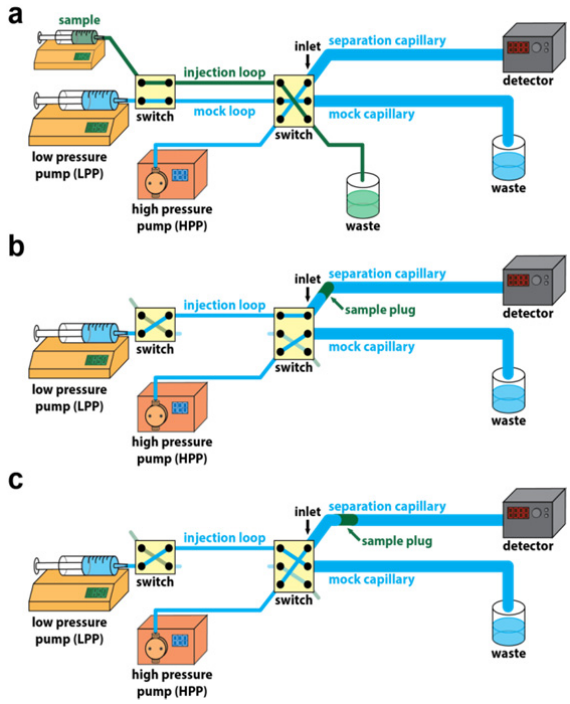

Schematic S1. Schematic of ACTIS fluidic system. **a)** Sample loading into the injection loop required for precisely dosing sample volume; LPP is pumping the buffer through a mock loop into a mock capillary, and HPP is pumping the buffer through the separation capillary. **b)** Transfer of the sample plug from the injection loop into the separation capillary by LPP using a low flow rate to maintain the near-cylindrical plug shape; the sample pump is idle (not shown), and HPP is pumping the buffer through the mock capillary. **c)** Propagation of the sample plug by HPP using a high flow rate and causing TIS of PL from L registered with a detector; the sample pump is idle (not shown), and LPP is pumping the buffer through the injection loop and the mock capillary. The mock loop and mock capillary mimic the injection loop and separation capillary, respectively, and allow LPP and HPP to run continuously under constant back-pressures.

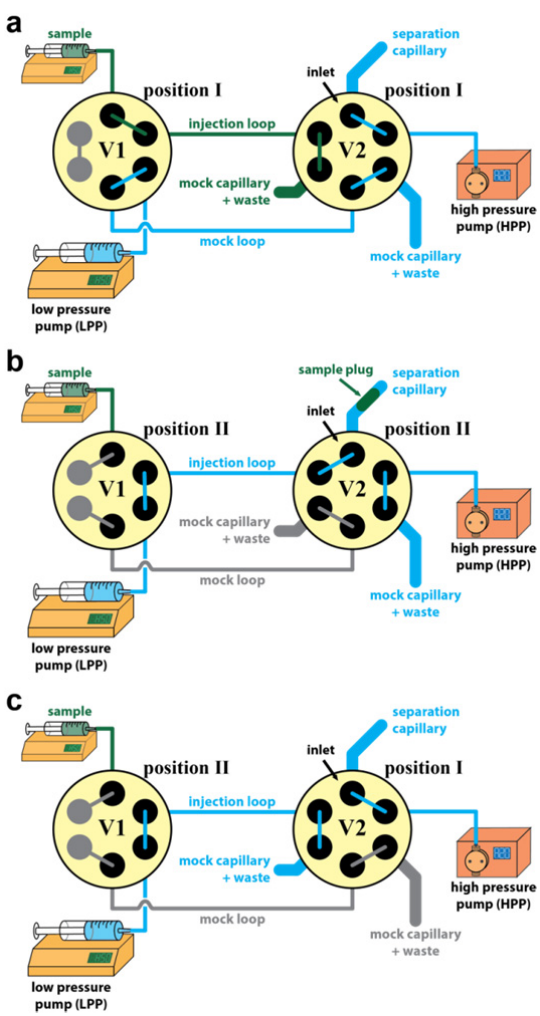

Schematic S2. Implementation of the two switches from Schematic S1 using two 6-port valves (V1 and V2). Note that for this implementation we used two mock capillaries which were identical in parameters and, therefore, are referred to as single one mock capillary throughout the manuscript for simplicity. Panels a–b of this schematic correspond to panels a–b in Schematic S1. Note that green, blue, and grey lines mark the EM sample, buffer, and lines/ports without flow, respectively. **a)** Sample loading: Filling the injection loop with the EM sample. At this stage, both valves (V1 and V2) are in position I. **b)** Sample transfer: Injection of the EM at a low flow rate followed by a plug of the buffer. At this stage, both valves (V1 and V2) are in position II. **c)** Sample propagation: Propagation of the EM at a high flow rate causing fast TIS of L from PL and P. At this stage, valve V1 is in position II and valve V2 is in position I.

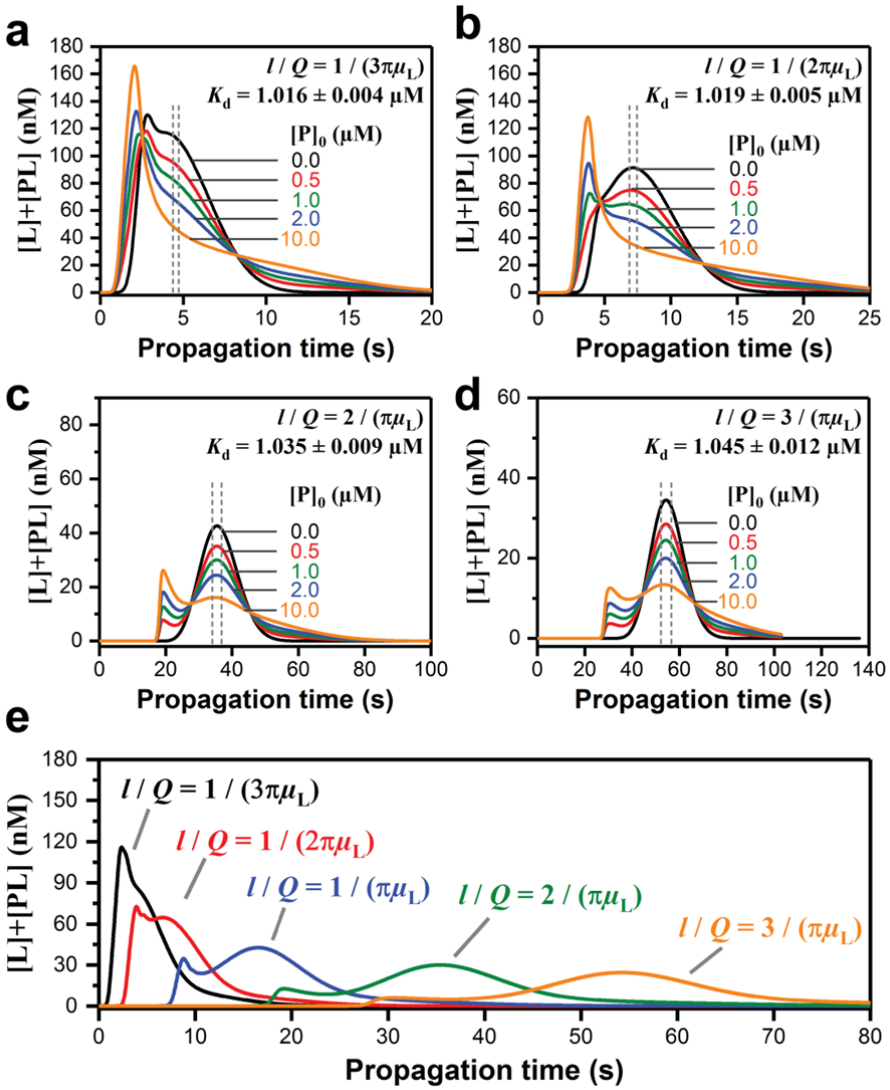

Figure S1. Influence of variation in l/Q on accuracy of ACTIS. Representative ACTIS separagrams for $[L]_0 = 0.5$ μM from a set of data in which $[P]_0$ ranges from 0 to $1000K_d$, $k_{off} = 10^{-3}$ s^{-1}, $k_{on} = 10^3$ M^{-1} s^{-1} ($K_d = k_{off}/k_{on} = 1$ μM), $\mu_L = 500$ μm^2/s, $\mu_P = \mu_{PL} = 50$ μm^2/s, internal capillary radius $a = 100$ μm, plug-injection flow rate = 0.1 μL/min, plug-injection time = 12 s, plug-transfer flow rate = 0.1 μL/min, plug-transfer time = 12 s, TIS flow rate $Q = 1$ μL/min. **a)** Separagrams for $l = 0.333$ cm. **b)** Separagrams for $l = 0.5$ cm. **c)** Separagrams for $l = 2$ cm. **d)** Separagrams for $l = 3$ cm. **e)** Separagrams for $[P]_0 = K_d$ for different l/Q; these separagrams are taken from panels a–d and presented in the same time scale.

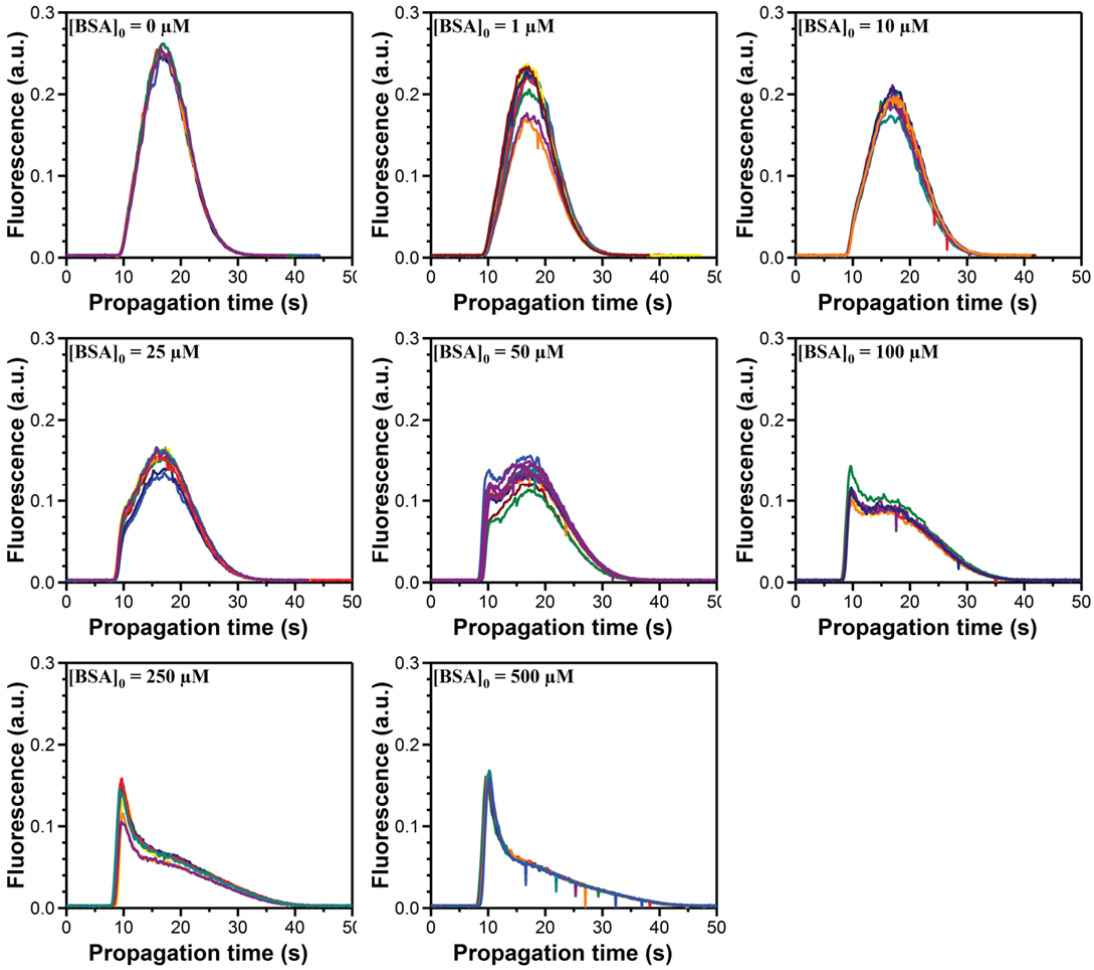

Figure S2. Repeatability of ACTIS separagrams for the BSA–fluorescein complex obtained with fluorescence detection with at least 7 repetitions at each $[BSA]_0$. Experimental conditions were: internal capillary radius a = 100 µm, inlet-to-detector distance l = 50 cm (full capillary length = 60 cm), injection loop's internal radius = 37.5 µm, injection loop's length = 22.7 cm (injection loop's volume = 1 µL), sample loading into the injection loop at a flow rate of 15 µL/min during 12 s, sample-plug transfer from the injection loop to the separation capillary at a flow rate of 5 µL/min during 24 s (plug length ≈ 3.2 cm, plug-end distance from the capillary inlet ≈ 3.2 cm), TIS flow rate Q = 50 µL/min, $[fluorescein]_0$ = 0.2 µM, $[BSA]_0$ ranged from 0 to 1 mM, the buffer was 30 mM ammonium acetate pH 7.5. Data shown is from the first experimental day; the repetition results from two next experimental days are similar (see raw data).

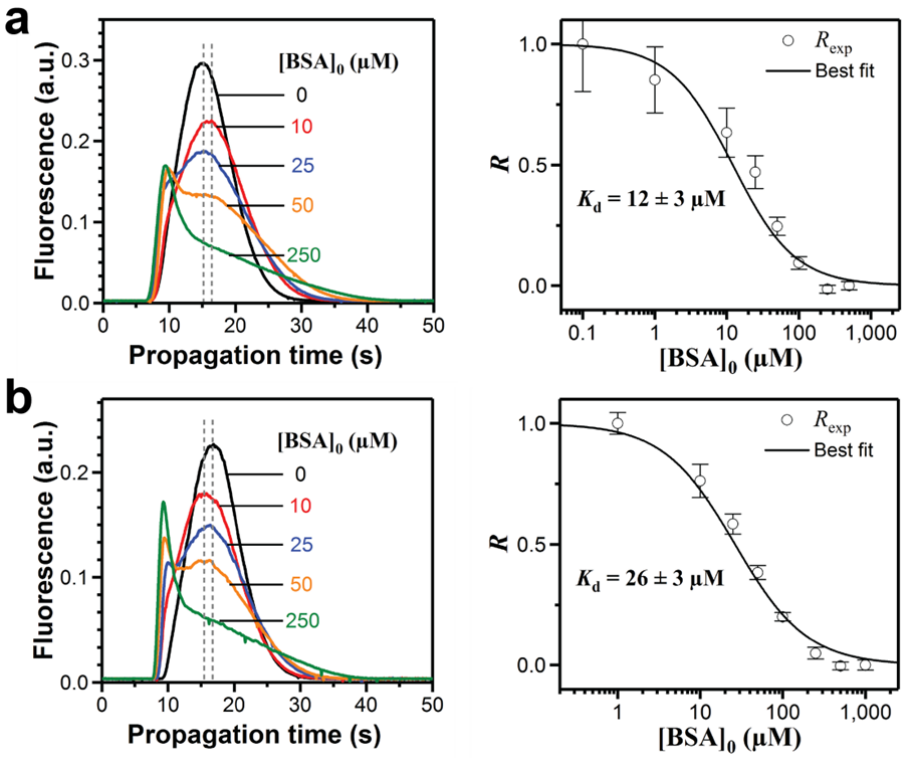

Figure S3. Reproducibility of K_d determination for the BSA-fluorescein complex by ACTIS. Binding isotherms R versus $[P]_0$ (open circles) and the best fit of the binding isotherm with Equation 6 from the main text (solid line). Experimental conditions were the same as in Figure 3 in the main text and in Figure S2. The uncertainty of R was obtained using Equation S24. **a)** Results for measurements (at least seven repetitions at each $[BSA]_0$) performed 4 days later than results shown in Figure 3. **b)** Results for measurements (at least five repetitions at each $[BSA]_0$) performed 19 days later than results shown in Figure 3.

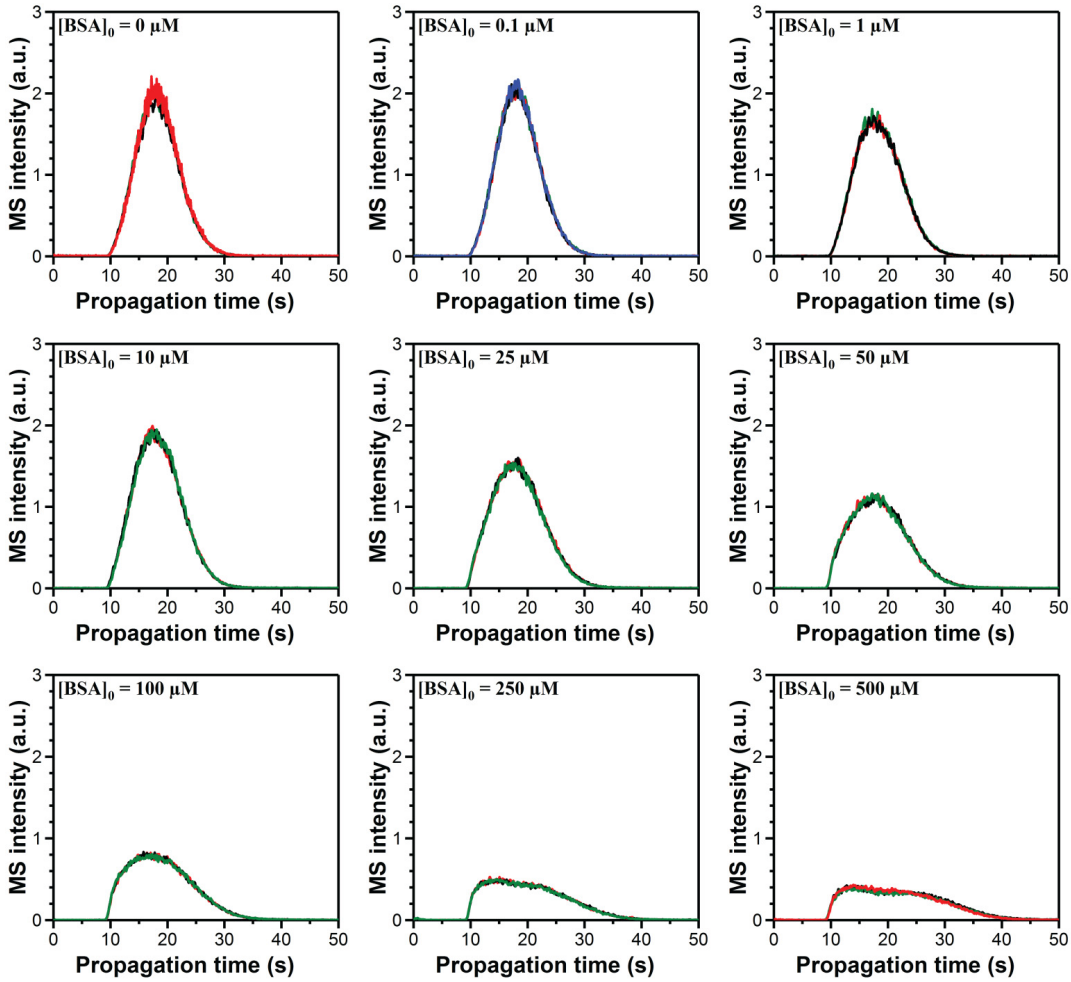

Figure S4. Repeatability of ACTIS separagrams for the BSA–fluorescein complex obtained with MS detection with at least three repetitions at each $[BSA]_0$. Experimental conditions were: internal capillary radius a = 100 μm, inlet-to-detector distance l = 100 cm (full capillary length = 100 cm), injection loop's internal radius = 37.5 μm, injection loop's length = 22.7 cm (injection loop's volume = 1 μL), sample loading into the injection look at a flow rate of 15 μL/min during 12 s, sample-plug transfer from the injection loop to the separation capillary at a flow rate of 5 μL/min during 24 s (plug length ≈ 3.2 cm, plug-end distance from the capillary inlet ≈ 3.2 cm), TIS flow rate Q = 100 μL/min, $[fluorescein]_0$ = 0.2 μM, $[BSA]_0$ ranged from 0 to 0.5 mM, the buffer was 30 mM ammonium acetate pH 7.5. MS experiments were carried with a QTRAP 6500+ instrument (AB Sciex, Concord, ON, Canada) utilizing a commercial Turbo V Atmospheric Pressure Chemical Ionization source. The optimal acceleration and focusing conditions were achieved by using a 60-V declustering potential at 525 °C and 90-psi gas pressure. The MS analysis was performed in the positive mode, and MS peak was detected at m/z = 287. The results were analyzed with Analyst QS 2.0 software. Data shown is from the first experimental day; the repetition results from the next experimental day are similar (see raw data).

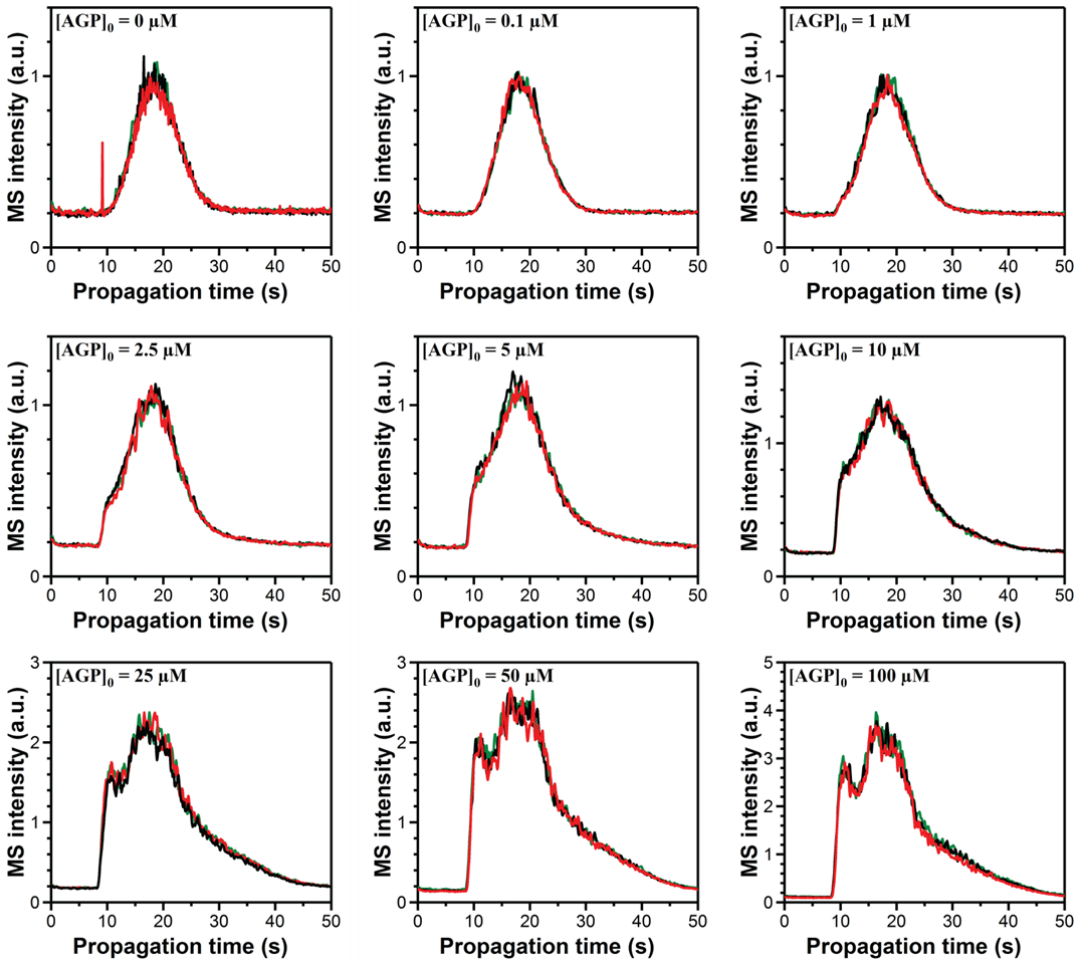

Figure S5. Repeatability of ACTIS separagrams for the AGP–alprenolol complex obtained with MS detection with at least three repetitions at each $[AGP]_0$. Experimental conditions were: internal capillary radius a = 100 µm, inlet-to-detector distance l = 100 cm (full capillary length = 100 cm), injection loop's internal radius = 37.5 µm, injection loop's length = 22.7 cm (injection loop's volume = 1 µL), sample loading into the injection loop at a flow rate of 15 µL/min during 12 s, sample-plug transfer from the injection loop into the separation capillary at a flow rate of 5 µL/min during 24 s (plug length ≈ 3.2 cm, plug-end distance from the capillary inlet ≈ 3.2 cm), TIS flow rate Q = 100 µL/min, $[alprenolol]_0$ = 0.5 µM, $[AGP]_0$ ranged from 0 to 0.2 mM, the buffer was 30 mM ammonium acetate pH 7.5. MS experiments were carried with a QTRAP 6500+ instrument (AB Sciex, Concord, ON, Canada) utilizing a commercial Turbo V Atmospheric Pressure Chemical Ionization source. The optimal acceleration and focusing conditions were achieved by using a 60-V declustering potential at 525 °C and 90-psi gas pressure. The MS analysis was performed in the positive mode, and MS peak was detected at m/z = 250. The results were analyzed with Analyst QS 2.0 software. Data shown is from the first experimental day; the repetition results from the next experimental day are similar (see raw data).

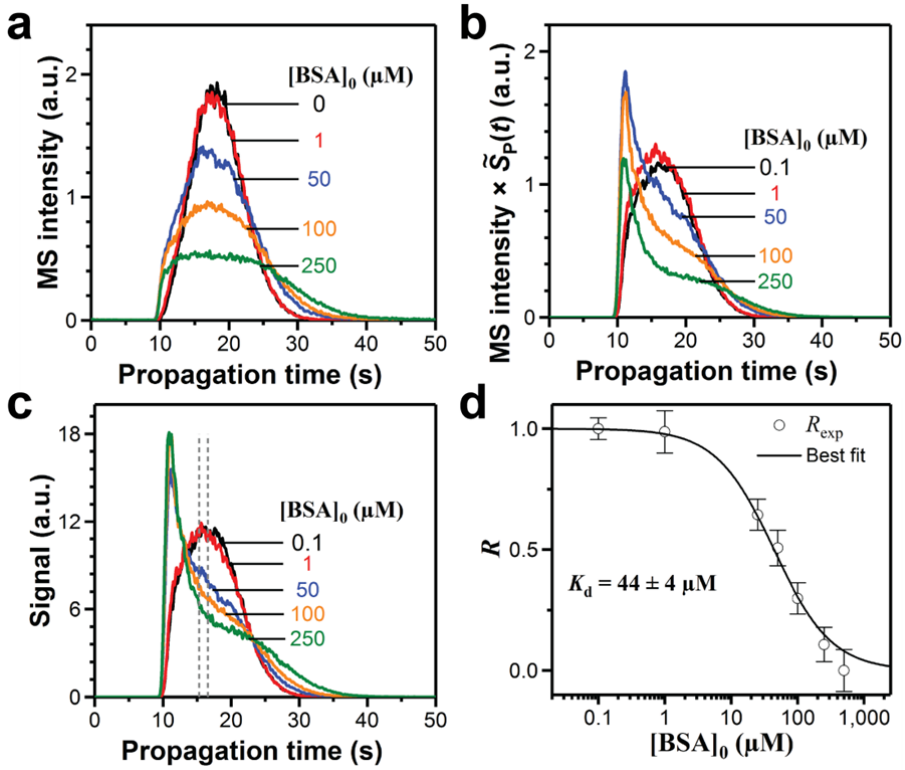

Figure S6. Use of the two-step signal correction procedure (unmasking) for ACTIS-MS of the BSA–fluorescein complex. **a)** Representative experimental separagrams, $S_{raw}(t)$, for $0 \leq [BSA]_0 \leq 10K_d$ to demonstrate the change in the separagrams with varying $[P]_0$. **b)** The result of the first step of correction, i.e. the multiplication product between $S_{raw}(t)$ and dimensionless simulated separagram of pure protein, $\tilde{S}_P$. **c)** The result of the second step of correction, i.e. fully corrected separagrams obtained by normalization of separagrams shown in panel (b) to the area under the separagram corresponding to the smallest $[P]_0 \neq 0$ (here: 0.1 μM). **d)** A binding isotherm R versus $[P]_0$ (open circles) obtained for the fully-corrected separagrams exemplified in panel (c) and the best fit of the binding isotherm with Equation 6 in the main text (solid line). The uncertainty of R was obtained using Equations S24 and S26. Experimental conditions were identical to those of experiments described in Figure S4.

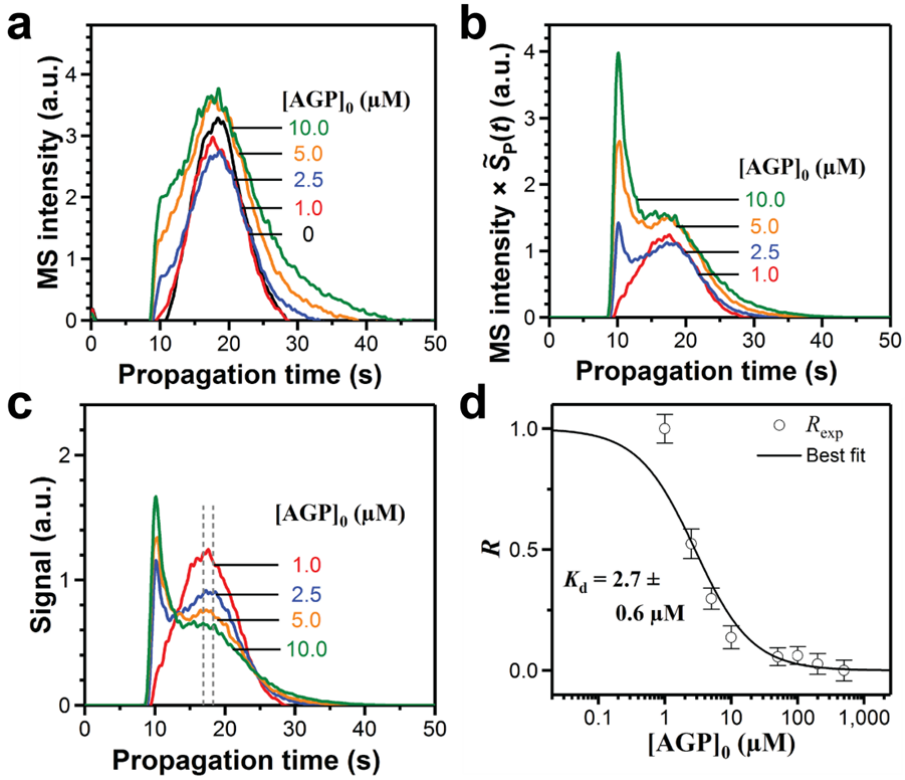

Figure S7. Use of the two-step signal correction procedure (unmasking) for ACTIS-MS of the AGP–alprenolol complex. **a)** Representative experimental separagrams, $S_{raw}(t)$, for $0 \leq [AGP]_0 \leq 10K_d$ to demonstrate the change in the separagrams with varying $[P]_0$. **b)** The result of the first step of correction, i.e. the multiplication product between $S_{raw}(t)$ and dimensionless simulated separagram of pure protein, $\tilde{S}_P$. **c)** The result of the second step of correction, i.e. fully corrected separagrams obtained by normalization of separagrams shown in panel (b) to the area under the separagram corresponding to the smallest $[P]_0 \neq 0$ (here: 1.0 μM). **d)** A binding isotherm R versus $[P]_0$ (open circles) obtained for the fully-corrected separagrams exemplified in panel (c) and the best fit of the binding isotherm with Equation 6 in the main text (solid line). The uncertainty of R was obtained using Equations S24 and S26. Experimental conditions were identical to those of experiments described in Figure S5.